19th Brazilian Congress of Thermal Sciences and Engineering
November 06th-10th, 2022, Bento Gonçalves - RS - Brazil

ENC-2022-0020
A CRITICAL EVALUATION OF FICK'S VERSUS STEFAN MAXWELL DIFFUSION MODELS TO PREDICT WAX DEPOSITION

Paulo Gustavo Cândido de Oliveira
Ivan Ibanez
Department of Mechanical Engineering – PUC-Rio, R. Marques de S. Vicente 225, Gávea, 22451-900, Rio de Janeiro, RJ, Brazil
paulogustavo17@gmail.com, iibanez@puc-rio.br

Felipe Fleming
Petrobras Brasileira S.A.
ffleming@petrobras.com.br

Luis Fernando A. Azevedo
Angela O. Nieckele
Department of Mechanical Engineering – PUC-Rio, R. Marques de S. Vicente 225, Gávea, 22451-900, Rio de Janeiro, RJ, Brazil
lfaa@puc-rio.br, nieckele@puc-rio.br

Abstract. *When hydrocarbons flow along pipelines losing heat to the environment, solid paraffin particles are formed when the temperature falls below a certain threshold known as wax appearance temperature (WAT). These particles can increase the viscosity, and they can also deposit on the inner walls of the pipelines, increasing the pumping power or completely obstructing the flow, resulting in a loss of several million dollars. Therefore, the ability to predict and control wax deposition in future events is important for designers and operators. The necessity of insulation and/or points for introducing PIGs to remove the deposit must be well planned by the pipeline designers, as well as the determination of proper frequency of wax mitigation techniques like mechanical removal or chemical treatment in offshore production. Although a large effort has been made by the scientific community aiming to improve the wax deposition prediction, most formulations are based on molecular diffusion models employing Fick's law, valid for binary mixtures. However, in the petroleum industry, the hydrocarbon flow is a multicomponent solution. In this article, a new approach based on the Maxwell-Stefan model, compatible with multicomponent diffusion systems is proposed. The Maxwell-Stefan formulation has larger applicability limits when compared with Fick's law, considering effects of complex interactions between the species. To determine the time and axial wax deposition thickness evolution, the flow was modelled as liquid/solid mixture and the conservation equations of energy, mass, linear momentum and species continuity were solved. The conservation equations were discretized with the finite volume method using the open-source software OpenFOAM®. In addition, the thermodynamic model employed is capable of predicting the growing and aging of the wax deposit with time and position. A critical evaluation of the performance of Fick and Maxwell-Stefan models is presented through comparison with experimental data.*

Keywords: *wax deposition, Maxwell-Stefan, Fick's law, pipeline, multicomponent diffusion*

1. INTRODUCTION

The wax deposition is one of the most challenging problems faced by the oil industry during the transportation and production in deep water. At high temperature, usually paraffin is soluble in crude oil, however, when the temperature falls below a certain threshold known as wax appearance temperature (WAT), the paraffin may precipitate out solution. The presence of the solid material may result in larger viscosity, increasing the head loss, forcing larger pumping power to maintain the same flow rate. More drastically, it can lead to total blockage of the duct, resulting in significant loss of production and capital. There are several approaches to remove the wax, like mechanical removal with PIGs or chemical treatment in offshore production, and determination of proper frequency of wax mitigation techniques is crucial. During the pipeline design, the necessity of insulation and/or points for introducing PIGs must also be well planned. For this reason, the ability to predict and control wax deposition is important for designers and operators. Nevertheless, several review studies have still been conducted in recent years, in order to contrast the different positions of the specialized community around the dominant mechanisms in the wax deposition process. For example, Liu *et al*. (2020); Ragunathan,

et al. (2020); Sousa *et al.* (2020) and van der Geest *et al*. (2021) discussed about several deposition mechanisms such as molecular diffusion, Soret diffusion, Brownian diffusion, gravity settling, shear dispersion, shear stripping and phase transition (heat transfer). Differently, in the review work carried out by Mehrotra *et al*. (2020), emphasis is made specifically on the heat transfer influence on the wax deposit growing.

The research effort to understand the wax deposition phenomenon has increased over time and has led to innumerous relevant works in literature. The scientific community directs efforts to identify the physical mechanisms that are relevant in the formation and growth process of wax deposit. Burger *et al*. (1981) was one of the first studies to discuss the influence of molecular diffusion on the wax deposition process. In this study, molecular diffusion is understood as the dominant mechanism. Over the years, Mehrotra's research group (Bidmus and Mehrotra, 2004; Ehsani and Mehrotra, 2019) has highlighted that the wax deposition phenomena is dominated by heat transfer. In the experiments conducted by Mehrotra's group, the temperature of the wax deposit interface remains equal to WAT. However, Linhares (2020) conducted a detail measurement of the interface temperature, and observed that initially the temperature is equal to the WAT and rapidly reaches a constant value between the WAT and the wax disappearance temperature (WDT). Linhares (2020) has also observed the presence of wax crystals locally in the solution at temperature above the WAT. Evidence from more recent studies (Veiga *et al.*, 2020 and Lee *et al.*,2020) seems to indicate that the growth and aging of the wax deposit are dominated by heat transfer and mass transfer, respectively. Seeking to model several physical phenomena (e.g. shear dispersion, molecular diffusion, heat transfer) that can influence the process of formation, growth and aging of the wax deposit, a robust mathematical model is needed. The referred robustness of the model must be able to solve the conservation equations (mass, momentum, species and temperature); constitutive equations (e.g.: viscosity and molecular diffusion coefficients of species) and state relations (thermodynamic model). Regarding conservation equations, the literature presents the enthalpy-porosity approach (Banki *et al*., 2008 and Veiga *et al.* 2020) and the multiple solid solutions model (Fleming, 2018). Concerning the resolution of state relations, there are three approaches in the literature: (Handsen *et al*., 1988; Lira-Galeana, 1996 and Coutinho *et al.* 2006a). With respect to constitutive equations, most authors have consider the fluid Newtonian (Matzaon, *et al.*, 2001; Fleming, 2018; Veiga *et al.*, 2020; Sulaimon *et al.*, 2020). In contrast, Zheng *et al*. (2017) models the fluid as a non-Newtonian fluid.

Still regarding the constitutive equations, to the best of the authors' knowledge, most mass diffusion models employed to determine the wax deposition phenomenon, found in the available literature, are based on Fick's law, which is valid for binary mixtures. However, it is well known, that most oils are formed by several hydrocarbons. Also, Agarwal *et al*., (2021) emphasizes the need to apply models capable of reproducing the mixture multicomponent diffusion. Therefore, in the present work, the mass diffusion flux is determined with Maxwell-Stefan model, which is compatible for multicomponent diffusion systems. To determine the flow field and wax deposition phenomenon, the flow was modelled as a liquid/solid mixture (Fleming, 2018). The solid precipitation and mixture properties were determined with the thermodynamic model of multiple solid solutions (Coutinho *et al.*, 2006). The conservation equations were numerically solved with the open-source software OpenFOAM®. A critical evaluation of the performance of Fick and Maxwell-Stefan models is presented through comparison with experimental data of Veiga *et al*. (2020).

2. DEPOSITION MODELING

The configuration considered is exactly the same as employed by Veiga *et al.* (2020), to allow for a direct comparison of the predictions with the experimental data. The setup is an annular duct with length L=1.05 m. The external pipe diameter is $D_{ex} = 2\ r_{ex}$ =19 mm, and the inner diameter is $D_{in} = 2\ r_{in}$ =34 mm, forming a radial gap of 7.5 mm ($gap = r_{ex} - r_{in}$), as shown in Fig. 1. Due to the angular symmetry of the configuration, the problem was modeled as 2D. A uniform velocity V_{in} was prescribed at the entrance of the test section. The inner pipe temperature $T_c\ (t)$ varied with time, and the experimentally measured value was imposed at the inner pipe. The external temperature T_{ex} was maintained at the same inlet temperature T_h, which was higher than Wax Appearing Temperature (WAT). The initial condition corresponded to a steady state situation with uniform temperature equal to T_h inside the whole domain since $T_c\ (t < t_o) = T_h$, where t_o is the initial of the deposition process, when a cooling ramp in the inner pipe was imposed, so that T_c reached a value below WAT (Fig. 1).

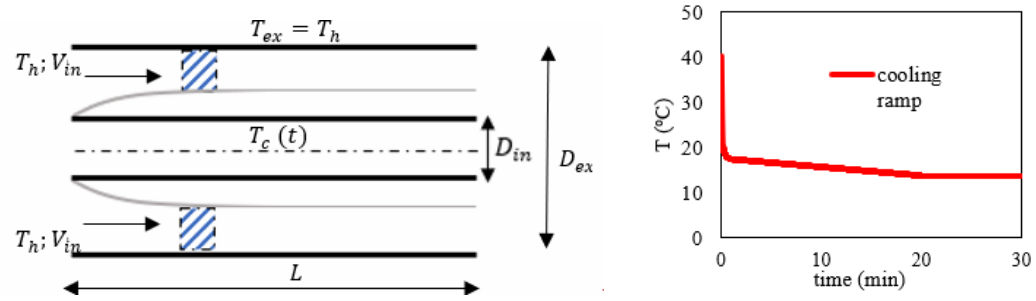

Figure 1. Domain of interest (annular pipe) and inner pipe, temperature ramp, $T_c\ (t)$.

The wax deposition model employed is based on the determination of the solid volume fraction S_s, assuming that the deposit was formed when the solid fraction was above 2%, as suggested by Holder and Winkler (1965). The wax solution was modeled as a Newtonian fluid mixture, formed by n =19 species (listed in Table 1), which can be present in both phases (solid and liquid). The mixture properties ϕ_m were defined as

$$\phi_m = S_s\phi_s + (1 - S_s)\phi_l \quad ; \quad S_s = \frac{\forall_s}{\forall_t} = \frac{B_s / \rho_s}{B_s / \rho_s + B_l / \rho_l} \tag{1}$$

where ϕ is a property obtained with the thermodynamic model of *Multiple Solid Solutions* (Coutinho *et al.*, 2006b) as a function of pressure p, temperature T and composition of the mixture z_i. ϕ can be density ρ, heat capacity c_p, thermal conductivity k, or viscosity μ (where the viscosity of the solid dissolved in the mixture is considered equal to the liquid viscosity). The subscript s and l correspond to solid and liquid phases. $\forall_s$ is the solid volume and $\forall_t$ the total volume. B_k and ρ_k are the mass fraction and specific mass of phase k, and are also determine with the thermodynamic model (Coutinho *et al.* 2006b). Details of thermodynamic model can be found in da Silva *et al.* (2017) and Fleming (2018).

The concentration of each specie i in the liquid and solid phase in the mixture are determined based on a Flash calculation, enforcing equilibrium between solid and liquid fugacity of each mixture specie i (da Silva *et al.*, 2017). Thus, when there is wax precipitation, the molar fraction of each specie i in each phase x_{ik} is obtained, and the total amount of molar fraction of species i (x_i), allowing to determine each phase properties and finally the mixture properties. As presented in Eq. (1), the solid volume fraction is determined from the mass fraction and specific mass of each phase. The density, thermal conductivity and viscosity are determined from the reduced properties as proposed by Queimada *et al.* (2005); Paradela *et al.* (2005) and Fleming (2018).

According to Fleming (2018), both phases velocities were defined as equal to the mixture velocity $\boldsymbol{u}_m$, while the mixture enthalpy h_m was mass based, $h_m = [(1 - S_s)\,\rho_l h_l + S_s \rho_s h_s]/\rho_m$. The flow was determined with the solution of the mixture conservation equations of mass, linear momentum, energy, and mass conservation of $n - 1$ species, since $\sum_{i=1}^{n} z_i = 1$.

$$\frac{\partial}{\partial t}(\rho_m) + \boldsymbol{\nabla}.(\rho_m \boldsymbol{u}_m) = 0 \tag{2}$$

$$\frac{\partial}{\partial t}(\rho_m \boldsymbol{u}_m) + \boldsymbol{\nabla}.(\rho_m \boldsymbol{u}_m \boldsymbol{u}_m) = -\boldsymbol{\nabla} p + \boldsymbol{\nabla} \cdot \boldsymbol{\tau}_m \quad ; \quad \boldsymbol{\tau}_m = \mu_m \left(\boldsymbol{\nabla} \boldsymbol{u}_m + \boldsymbol{\nabla}^T \boldsymbol{u}_m - \frac{2}{3} \nabla.\boldsymbol{u}_m \boldsymbol{I}\right) \tag{3}$$

$$\frac{\partial}{\partial t}(\rho_m h_m) + \nabla.(\rho_m h_m \boldsymbol{u}_m) = -\nabla \cdot \boldsymbol{q} \; ; \quad \boldsymbol{q} = -k_m \boldsymbol{\nabla} T + \sum_{i=1}^{N} \boldsymbol{j}_i \, h_i \tag{4}$$

$$\frac{\partial}{\partial t}\left(\rho_{m,i}\right) + \boldsymbol{\nabla}.\left(\rho_{m,i} \boldsymbol{u}_m\right) = -\boldsymbol{\nabla} \cdot \boldsymbol{j}_i \tag{5}$$

where $\rho_{m,i}$ are the mass fraction of species i. $\boldsymbol{\tau}_m$ and $\mathbf{q}$ are the viscous stress and diffusive heat flux, respectively. $\boldsymbol{j}_i$ are the species i diffusive mass flux, which is described in detail in the next sub-section.

Table 1. Species molar concentration of the solution at the inlet.

Carbon number	Molar composition, (z_i)	Carbon number	Molar Composition, (z_i)
C_{12}	9.03×10^{-1}	C_{31}	7.20×10^{-3}
C_{22}	6.61×10^{-5}	C_{32}	4.63×10^{-3}
C_{23}	4.59×10^{-4}	C_{33}	2.91×10^{-3}
C_{24}	2.49×10^{-3}	C_{34}	1.81×10^{-3}
C_{25}	7.00×10^{-3}	C_{35}	1.13×10^{-3}
C_{26}	1.21×10^{-2}	C_{36}	7.20×10^{-4}
C_{27}	1.56×10^{-2}	C_{37}	4.71×10^{-4}
C_{28}	1.60×10^{-2}	C_{38}	3.16×10^{-4}
C_{29}	1.38×10^{-2}	C_{39}	2.07×10^{-4}
C_{30}	1.05×10^{-2}		

2.1. Mass Transfer

Two mass diffusion models were considered here. The first one is the Fick´s model which is defined for binary mixtures and second one is the Stefan-Maxwell model compatible for multicomponent mixtures (Krishna and Wesselingh, 1997).

Fick's law proposes a linear dependence of the diffusive flux $\boldsymbol{j}_i$ and the species molar fraction gradient $\boldsymbol{\nabla} x_i$, assuming the fluid as a binary mixture, diffusing dilute species i in a multicomponent system and in the absence of electrostatic or centrifugal force fields (Krishna and Wesselingh, 1997). Fleming (2018) proposed to simplify the model, considering that the solid diffusion is null and only the diffusion between the solvent (C_{12}) and each species i is relevant. The simplified Fick diffusion model was select here, to represent the mass diffusion flux

$$\boldsymbol{j}_i = -D_i \boldsymbol{\nabla} c_{i,l}\, S_l\, \rho_l \quad ; \quad c_{i,l} = x_{i,l} \frac{MM_i}{MM_l} \tag{6}$$

where MM_i and MM_l are, respectively, the molar mass of species i and the molar mass of the liquid phase. D_i is the Fick's binary diffusion coefficient between the solvent (C12) and each species i. In this modified Fick diffusion model D_i is equal to the diffusion coefficients at infinite dilution (D_i^0). Here, D_i was determined with the correlation of Hayduk and Minhas (1982) in m^2/s as

$$D_i = Đ_{i12} = Đ_{i12}^o = 13.3 \times 10^{-4}\, T^{1.47} \mu_{C12}^{\left(\frac{10.2}{V_i} - 0.791\right)} V_i^{-0.71} \tag{7}$$

where T is the temperature in K; V_i is the molar volume of each species i in cm^3/mol and μ_{c12} is the solvent viscosity in $mPa\ s$.

The diffusive mass flux of the Stefan Maxwell model is

$$\boldsymbol{j}_i = -MM_i\ C_m\, \boldsymbol{B}^{-1}\, \boldsymbol{d_i} \quad ; \quad C_m = \sum_{i=1}^{N} C_i \quad ; \quad C_i = \frac{\rho_i}{MM_i} \quad ; \quad \boldsymbol{d_i} = \sum_{j=1}^{n-1} \Gamma_{ij}\, \boldsymbol{\nabla} x_j \quad ; \tag{8}$$

where C_m is the mixture molar concentration, the matrix $\boldsymbol{B}$ is related to the diffusion coefficients and $\boldsymbol{d_i}$ is the driving force, based on a non-ideal thermodynamic factor $\boldsymbol{\Gamma}$, which depends on γ_i, the activity coefficient of each species i. The components of the matrix $\boldsymbol{B}$ and $\boldsymbol{\Gamma}$ (where the repeated index does not imply sum) are

$$\Gamma_{ij} = \delta_{ij} + x_i \frac{\partial \ln \gamma_i}{\partial x_j} \quad ; \quad B_{ii} = \frac{x_i\, MM_i}{Đ_N MM_N} + \sum_{\substack{k=1 \\ k \neq i}}^{n} \frac{x_k}{Đ_{ik}} \qquad B_{ij} = -x_i \left(\frac{1}{Đ_{ij}} - \frac{MM_j}{Đ_{iN} MM_N} \right) \tag{9}$$

The Stefan Maxwell diffusion coefficient $Đ_{ij}$ is estimated based in a multicomponent correlation (Wesselingh and Krishna, 1990) as a function of the binary ideal diffusion coefficient $Đ_{ij}^o$, which is given by the correlation of Hayduk and Minhas (1992) between species i in relation to species j

$$Đ_{ij} = (Đ_{ij}^o)^{\frac{1+x_j-x_i}{2}}\ (Đ_{ji}^o)^{\frac{1+x_i-x_j}{2}} \qquad ; \quad Đ_{ij}^o = 13.3 \times 10^{-4}\ T^{1.47} \mu_j^{\left(\frac{10.2}{V_i} - 0.791\right)} V_i^{-0.71} \tag{10}$$

2.2. Numerical method

The numerical method designate for solving the governing equations was the finite volume method (Versteeg and Malalasekera, 2007, Patankar, 1980) with the software OpenFOAM®, an opensource software for computational fluid dynamics. To solve the discretized equations the second order linear Upwind method was selected for solve the convective terms, the central difference scheme was chosen for solving the diffusive terms and the second order backward scheme to solve the temporal discretization. The set of conservation equation were solved in a sequential order, according to method SIMPLE a global conference was implemented in order to ensure a minimum tolerance between the mass fraction calculated using the thermodynamic model and the species mass conservation equations.

3. RESULTS

Figure 2 presents a comparison of the deposit thickness obtained with both diffusion models (simplified Fick and Stefan Maxwell) along the test section, for different time instants and compares with the experimental data of Veiga *et al.* (2020). Until twenty minutes no different between the predictions of both models has been observed.

Besides the deposit thickness, Veiga *et al.* (2020) measured the radial temperature profile at z/L=0.75, near the test section exit. Figure 3 illustrates the radial temperature profile at z/L=0.75, obtained with both diffusion models, at the begging of the deposition process, t=5mim. To aid the analysis of the figure, the measured and predicted deposit thickness is also included in the figure. For this position and time, both models predicted exactly the same thickness and although they are slightly different then the experimental data result, the radial temperature profile of both models present good agreement with experimental data.

At the same axial position, z/L=0.75, it is shown in Fig. 4, the numerical predicted radial mass fraction profile of the solvent C_{12}, at t= 20 mim. The initial mass fraction is also indicated as a dotted line. Once again, the deposit thickness numerical is indicated in the figure. Note that inside the deposit the solvent concentration is reduced, with position of the minimum value slightly displaced from the cold wall. The Stefan-Maxwell model shows a slightly stronger variation of

the solvent profile along the cross section, with smaller C_{12} values. Near the deposit interface, both models predicted similar results, with a small increase of C_{12} concentration in relation to the initial concentration.

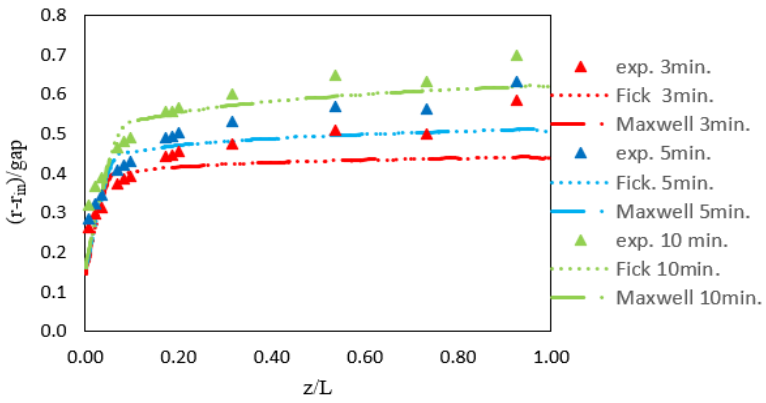

Figure 2. Deposit thickness along test section at different time instants.

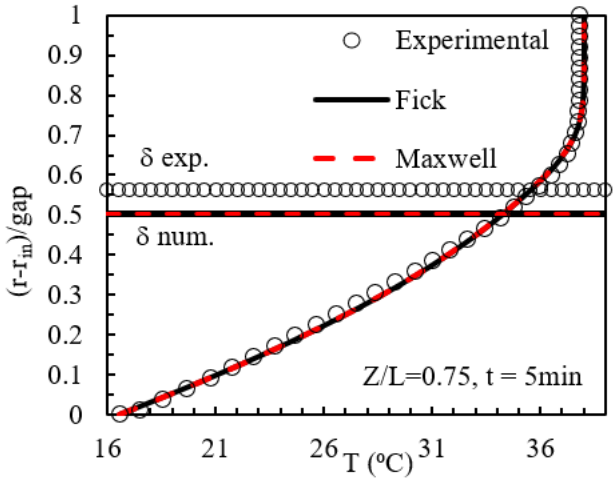

Figure 3. Radial temperature profile at z/L=0.75, t=5 mim.

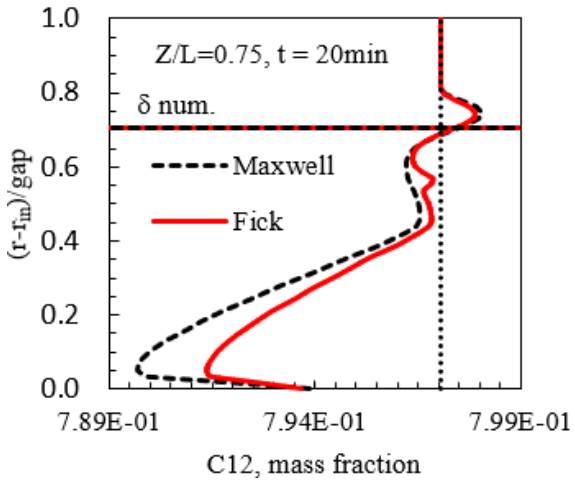

Figure 4. Radial mass concentration profile of the solvent C_{12} at z/L=0.75, at t=20 min.

Six different solutes were selected to be analyzed in more detail, i.e., their radial mass fraction profile at t=20 min, and z/L=0.75 obtained with both models are shown in Fig. 5. The lighter solutes, C_{22} and C_{23} present a profile similar to C_{12}. Smaller reduction of the mass concentration was obtained with Stefan-Maxwell model, and no mass fraction increase was obtained above the deposit interface. As the number of carbons increase, a change is observed to the radial profile, but both models still predict the same behavior, with differences inferior to 1% in relation to their respective initial

concentration and, reduction of the mass fraction is seen for both models above the deposit interface. C_{38} and C_{39} present equivalent radial profile, with a mass fraction increase in relation the initial concentration, not only near the cold wall, but near the deposit interface. C_{28} is the component of the solute with the largest concentration. Its radial profile is quite different from the others solute components, with a reduction of its mass concentration near the deposit interface, and an increase near the cold wall. For C_{34}, the reduction of its concentration in relation to its initial value occurs only above the deposit interface, with larger values inside the deposit.

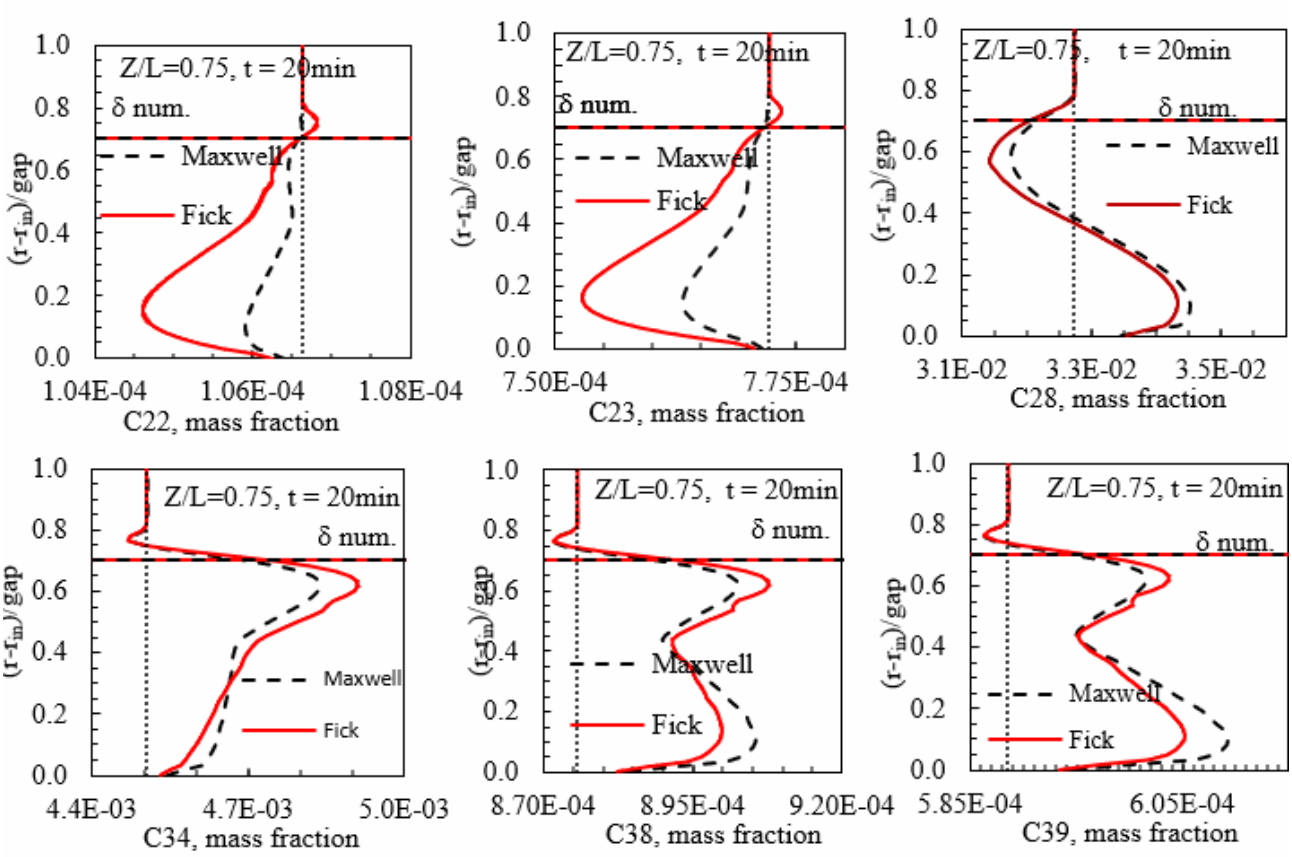

Figure 5. Radial mass fraction profile at z/L=0.75 , at t=20 min of six solutes (C_{22}, C_{23}, C_{28}, C_{34}, C_{38} and C_{39}).

To evaluate the time evolution during the deposition process, it is shown in Fig. 6, the radial mass fraction of three solutes (C_{22}, C_{28}, and C_{34}), at three time instants (5 min; 10 min and 20 min), at z/L=0.75. For all three species, as time evolves, stronger variations along the cross section is observed, with very similar profiles for both models, although Fick´s models predicts larger non-uniformities of the mass fraction. It can be seen, larger reduction of the lighter solute (C_{22}) inside of the deposit as oppose to an increase of the heavier species, as time increases. However, it should be noted that as time increases, the maximum differences between the mass fraction predicted by Fick´s models and Stefan-Maxwell model become greater, i.e., 0.77 % at 5 mins; 1.10% at 10 mins and 1.70% at 20 mins.

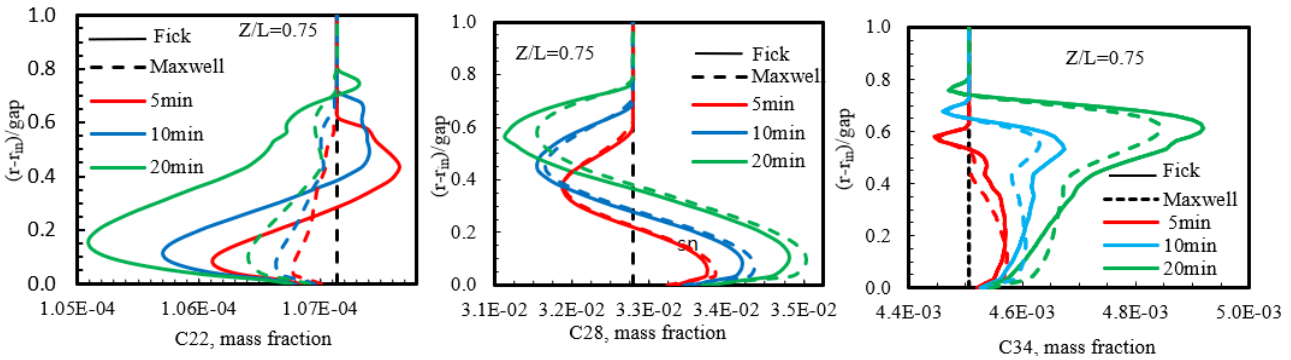

Figure 6. Radial solute mass concentration profile at z/L=0.75, at different time instants. (C_{22}, C_{28} and C_{34}).

Figure 7 shows the radial profile of each model diffusion coefficient at z/L=0.75 and t=20 min. Figure 7a shows the binary diffusion coefficient $Đ^{o}_{i12}$ (Eq. 7) of all components in relation with the solvent C_{12}, as employed in Fick´s model. It is observed an increase in diffusion coefficient as the carbon number increases, and larger diffusion coefficient at the warmer region, near the external wall. The same is observed in Fig. 7b, for the multicomponent diffusion coefficient $Đ_{ij}$ (Eq. 11) employed to determine the diffusion flux of the Stefan Maxwell model. However, in this case, it is shown the diffusion coefficient $Đ_{ij}$ of C_{22} and C_{34} in all other species. In Fig 7b, it can be clearly seen that the diffusion to the solvent C_{12} is significant larger, indicating that the simplified Fick´s models that only consider diffusion to the solvent is a good approximation.

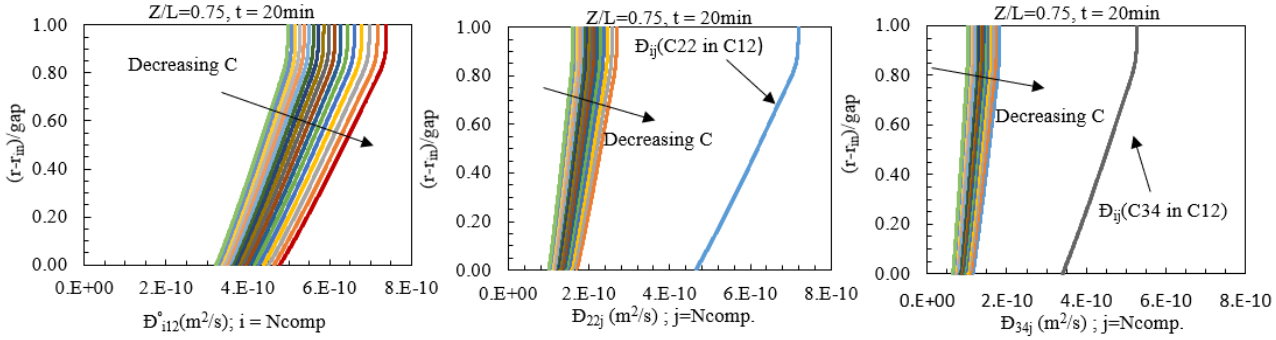

(a) Fick´s model (b) Stefan-Maxwell model. $Đ_{ij}$ for i= C_{22} and C_{34}

Figure 7. Radial diffusion coefficient at z/L=0.75 , at t=20 min, a) Fick´s model b) Stefan-Maxwell model

Figure 8 shows a direct comparison of the radial distribution of the diffusion coefficient of C_{22} and C_{39} in the solvent C_{12} based on Fick´s model and Stefan-Maxwell model at z/L=0.75 and t=20 min. The maximum difference of the diffusion coefficient in relation to Ficks´s model was 2.8% for the C_{22} and 4.4% for the C_{39}. This small difference explains the similarity of the previous results not only for the mass fraction of different species, but for the deposit thickness. The present results indicates that during the begging of the deposition process the hypothesis of a thermodynamically ideal mixture of Fick´s model is reasonable, since the thermodynamic factor Γ of Maxwell-Stefan model is close to 1.

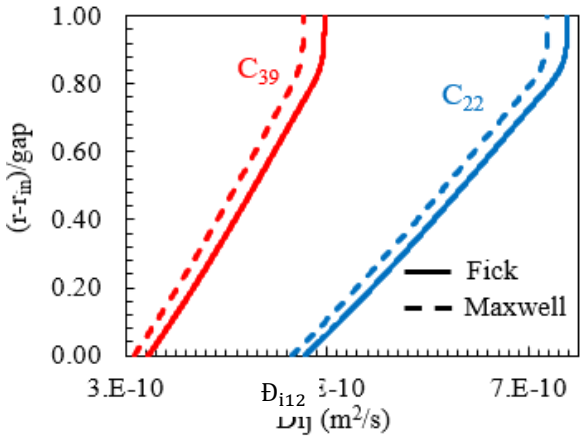

Figure 8. Radial binary diffusion coefficient of C_{22} and C_{39} in C_{12}, for Fick´s and Stefan-Maxwell models at z/L=0.75 , at t=20 min

To aid in the analysis of the impact of the diffusion mass flux model in the deposition phenomena, the forcing to the mass species concentration equation (Eq. 5), the divergence of the mass flux of species i ($\nabla \cdot \boldsymbol{j}_i$) is analyzed, for the same previously selected species. A positive value of $\nabla \cdot \boldsymbol{j}_i$ indicates a sink of the species and a negative value a source. The radial profile of this forcing is shown in Fig. 9 at z/L=0.75 , at t=20 min. As expected, the results show a direct connection between of the divergence of the mass diffusion flux and the mass fraction distribution, for the examined models. The simplified Fick´s model only considers the diffusion to the solvent, resulting in a source of C_{22} and C_{23} above the deposit interface, while in Stefan-Maxwell model, the diffusion to all other species is accounted for, resulting in a sink of the referred species above the deposit interface. However, note that the resulting mass flux forcing of these two lighter species is significantly smaller than for the heavier components. For the heavier species, both fluxes are almost identical, indicating that the mayor contribution to the mass flux is indeed to the solvent.

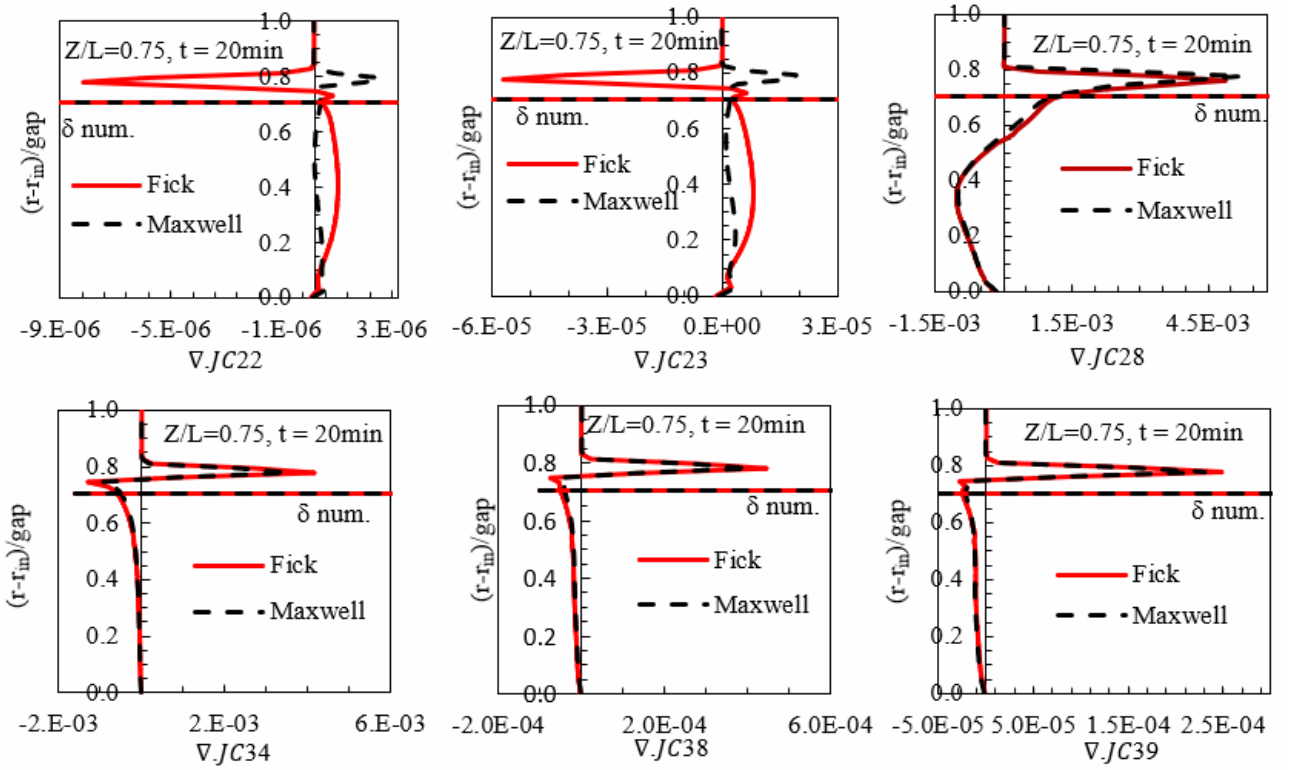

Figure 9. Forcing of species concentration, divergence of the mass diffusion flux $\nabla \cdot \boldsymbol{j}_i$, for C_{22}, C_{23}, C_{28}, C_{34}, C_{38} and C_{39} at z/L=0.75 , at t=20 min.

4. CONCLUSION

The present work investigates the impact of Stefan Maxwell and Fick's diffusion models on wax deposition phenomena. The differences between the models were identified through the analysis of the deposit thickness, temperature profiles; mass fractions of each species, diffusion coefficient of each species and divergent of mass diffusive flux.

Both models predicted very similar results for the beginning of the deposition process, showing enhancement of the heavy species and decrease of the lighter ones inside the deposit, as time evolves.

It was shown that the diffusion coefficient associate with the solvent C_{12} is indeed dominant, what explains the small different between the models. This could lead the hypothesis that the simplified Fick´s model (based on a thermodynamically ideal mixture) is sufficient to predict the wax deposition. Nevertheless, it is necessary to compare the mass fraction results with experimental data, and to evaluate longer deposition times, specially, after the deposit stops growing, but the hardening (aging) of the deposit occurs.

5. ACKNOWLEDGEMENTS

The authors thank the Brazilian Government agencies CAPES and CNPq for the continuous support, and to Petrobras and TotalEnergies in Brazil for their support to carry out this present work.

6. REFERENCES

Agarwal, J. R., Torres, C.F. and Shah, S., 2021. "Development of dimensionless parameters and groups of heat and mass transfer to predict wax deposition in crude oil pipelines." *ACS Omega*, Vol. 6, pp. 10578−10591

Banki, R., Hoteit, H. and Firoozabadi, A., 2008. "Mathematical formulation and numerical modeling of wax deposition in pipelines from enthalpy-porosity approach and irreversible thermodynamics". *International Journal of Heat and Mass Transfer*, Vol. 51, pp. 3387-3398.

Burger, E. D., Perkins, T. K. and Striegler, J. H., 1981. "Studies of waxdeposition in the trans alaska pipeline". *Journal of Petroleum Technology*, pp. 1075–1086.

Bidmus, H. O. and Mehrotra, A. K., 2004. "Heat-transfer analogy for wax deposition from paraffinicmixtures". *Industrial & Engineering Chemistry Research*, Vol. 43, No. 3, pp. 791-803.

Ehsani, S. and Mehrotra, A. K., 2019. "Validating heat-transfer-based modeling approach for wax deposition from paraffinic mixtures: an analogy with ice deposition. *Energy & Fuels*, Vol. 33, No. 3, pp. 1859-1868.

Coutinho, J. A. P.; Edmonds, B; Moorwood, T.; Szczepanski, R.; Zhang, X. 2006a, "Reliable wax predictions for flow assurance". *Energy & Fuels*, Vol. 20, No. 3, pp. 1081-1088.

Coutinho, J. A., Mirante, F., and Pauly, J., 2006b. "A new predictive UNIQUAC for modeling of wax formation in hydrocarbon fluids". *Fluid Phase Equilibria*, Vol. 247, No. 1-2, pp. 8-17.

da Silva, V. M.; do Carmo, R.P., Fleming, F.P., Daridon, J., Pauly, J. and Tavares, F.W., 2017. "Paraffin solubility and calorimetric data calculation using Peng-Robinson EoS and modified UNIQUAC models. *Journal of Petroleum Science and Engineering*, Vol. 156, pp. 945-957.

Fleming, F. P., 2018. "Fundamental study of wax deposition under real flow conditions". *D.Sc. thesis*, Mechaning Eng., PUC-Rio.

Hansen, J.H., Fredenslund, A., Pedersen, K.S. and Ronningsen, H.P., 1988. "A thermodynamic model for predicting wax formation in crude oils". *AICHE Journal*, Vol. 34, No. 12, p. 1937-1942.

Hayduk, W. and Minhas, B., 1982. "Correlations for prediction of molecular diffusivities in liquids". *The Canadian Journal of Chemical Engineering*, Vol. 60, No. 2, pp. 295-299.

Holder, G. and Winkler, J., 1965. "Wax crystallization from distillate fuels". *Journal Inst. Pet*., Vol. 51, No. 499, pp. 228-252.

Krishna, R. and Wesselingh, J., 1997, "The Maxwell-Stefan approach to mass transfer. Chemical engineering science, Vol. 52, No. 6, pp. 861-911.

Linhares, R., 2020. *Wax deposits formation in petroleum pipelines: investigation of the deposit-liquid interface characteristics*. Masters Dissertation, Department of Mechanical Engineering, Pontifical Catholic University of Rio de Janeiro (PUC-Rio), Rio de Janeiro, RJ, Brasil.

Lee, J., Mahir, L. H. A. and Larson, R. G. (2020). Experimental Investigation of Time-Dependent Thickness and Composition of Multicomponent Wax Deposits on Cold Surfaces. *Energy & Fuels*, Vol. 34, No. 10, pp.12330-12339.

Lira-Galeana, C.; Firoozabadi, A. and Prausnitz, J. M., 1996. "Thermodynamics of wax precipitation in petroleum mixtures". *AICHE Journal*, Vol. 42, No. 1, pp. 239-248.

Liu, Z., Li, Y., Wang, W., Song, G., Lu, Z. and Ning, Y.,. 2020. "Wax and wax–hydrate deposition characteristics in single, two-, and three-phase pipelines: A review". *Energy & Fuels*, Vol. 34, No. 11, pp. 13350-13368.

Matzain, A., Apte, M.S., Zhang, H., Volk, M., Redus, C.L., Brill, J.P. and Creek, J.L. 2001, "Multiphase flow wax deposition modeling". In *Proceedings of the ASME 2001 Engineering Technology Conference on Energy*. *Part B: Offshore and Arctic Operations; Pipeline Technology; Production Technology; Tribology*. Houston, Texas, USA. pp. 927-937.

Mehrotra, A. K., Ehsani, S., Haj-Shafiei, S. and Kasumu, A. S. 2020. "A review of heat-transfer mechanism for solid deposition from waxy or paraffinic mixtures". *The Canadian Journal of Chemical Engineering*, Vol. 98, No. 12, pp. 2463- 2488.

Paradela, F., Queimada, A., Marrucho, I., Neto, C., and Coutinho, J., 2005. "Modeling the thermal conductivity of pure and mixed heavy n-alkanes suitable for the design of phase change materials". *International Journal of Thermophysics*, Vol. 26, No. 5, pp. 1461-1475.

Patankar, S., 1980. *Numerical heat transfer and fluid flow*. CRC Press, 1a Ed.

Queimada, A. J., Marrucho, I. M., Coutinho, J. A. P. and Stenby, E. H., 2005. "Viscosity and liquid density of asymmetric n-Alkane mixtures: Measurement and modeling". *International Journal of Thermophysics*, Vol. 26, No. 1, pp. 47–61.

Ragunathan, T., Husin, H. and Wood, C.D., 2020. "Wax formation mechanisms, wax chemical inhibitors and factors affecting chemical inhibition." *Applied Sciences*, Vol. 10, No. 2, pp 479-497.

Sousa, A. M., Matos, H. A. andGuerreiro, L., 2020. "Wax deposition mechanisms and the effect of emulsions and carbon dioxide injection on wax deposition: Critical review". *Petroleum*, Vol. 6, No. 3, pp.215-225.

Sulaimon, A. A., Gunasekaran, K. and Vatsa, S., 2020. "Evaluating the mechanisms of wax deposition in crude oil pipelines". *Platform: A Journal of Engineering*, Vol. 4, No. 3, pp. 1-10.

Van der Geest, C., Melchuna, A., Bizarre, L., Bannwart, A. C. and Guersoni, V. C., 2021. "Critical review on wax deposition in single-phase flow". *Fuel*, Vol. 293, pp. 120358.

Veiga, H. M., Boher e Souza, L., Fleming, F. P., Ibanez, I., Linhares, R. C., Nieckele, A. O. and Azevedo, L. F. A., 2020. " Experimental and Numerical Study of Wax Deposition in a Laboratory-Scale Pipe Section under Well-Controlled Conditions". *Energy & Fuels*, Vol. 34, No. 10, pp. 12182-12203.

Versteeg, H. and Malalasekera, W., 2007. *An introdution to computational fluid dynamics*. *The finite volume method*. Prentice Hall, 2nd Ed.

Wesselingh, J. and Krishna, R., 1990. *Mass transfer*. Ellis Horwood London.

Zheng, S., Saidoun, M., Palermo, T., Mateen, K. and Fogler, H.S., 2017. "Wax deposition modeling with considerations of non-newtonian characteristics: application on field-scale pipeline." *Energy & Fuels*, Vol. 31, No. 5, pp. 5011-5023.

7. RESPONSIBILITY NOTICE

The authors are the only responsible for the printed material included in this paper.